

Imaging Algorithms for Locating Damage via *in situ* Ultrasonic Sensors

Jennifer E. Michaels¹, Anthony J. Croxford² and Paul D. Wilcox²

¹School of Electrical and Computer Engineering, Georgia Institute of Technology, Atlanta, Georgia, 30332-0250, USA
Phone: 1-404-894-2994, Email: jennifer.michaels@ece.gatech.edu

²Department of Mechanical Engineering, University of Bristol, Bristol, BS8 1TR, UK

Abstract – Permanently mounted ultrasonic sensors arranged as a spatially distributed array are being considered for *in situ* monitoring of the integrity of structural components. Here we consider two imaging algorithms for locating damage based upon changes in received signals. All transducer pairs in the array are considered, with each transducer acting in turn as a transmitter and the remaining transducers as receivers. The first imaging algorithm is based upon spatially distributing the differenced signals between each transducer pair as per expected arrival times for discrete scatterers. The resulting images, which consist of concentric ellipses, are summed over all pairs to form the final image. The second algorithm is based upon the cross correlation between waveforms originating from the same transmitter and received by two different transducers. The cross correlation waveforms, which capture the time difference of arrival between two pairs, are similarly distributed and summed to form the final image via a hyperbolic rather than an elliptical relationship. Results are shown for artificial damage in an aluminum plate.

Keywords – structural health monitoring, acoustic arrays, acoustic imaging, acoustic signal processing.

I. INTRODUCTION

Ultrasonic methods are being considered to monitor the integrity of critical structures such as airplanes, bridges and buildings because they are one of the few, if only, techniques which can interrogate large areas and maintain sensitivity to damage. A spatially distributed array of piezoelectric sensors, with each able to act as transmitter or receiver, is one possible configuration. Signals between multiple transducer pairs can be continuously or periodically monitored with the goal of detecting and locating damage based upon changes in the monitored signals over time.

Here we consider the problem of localizing the damage once it has been detected. One type of algorithm is based upon a “damage index,” which is some measure of how different the current signal is from a baseline signal. Damage indexes for all transducer pairs are spatially distributed and summed to generate an image of the damaged area [1]. A second algorithm is of the “delay-and-sum” type whereby differenced signals from all transducer pairs are delayed and summed for each spatial point in the image [2,3,4]. At locations of actual damage, scattered arrivals thus reinforce

and are visible as higher intensity regions on the image. A third type of algorithm constructs a composite feature at each spatial location from all signal pairs based upon the energy distribution in the neighborhood of calculated arrival times [5]. All of these algorithms utilize the fact that active ultrasonic signals are repeatable and the time origin of the excitation is known.

The more general problem of locating acoustic sources using passive sensors has the additional complication of an unknown time origin of the source. Algorithms based upon the time difference of arrival between multiple sensors are thus commonly used for source location, provided that the signals received are coherent and a time difference can be estimated [6,7]. These types of algorithms are typically used for locating acoustic emission sources [8,9].

II. ANALYSIS

Described here are first the preprocessing steps applied to the received signals, and then the two damage location algorithms based upon the difference of signals recorded before and after introduction of damage. The drawing of Fig. 1, showing a spatially distributed array of three transducers, applies to both algorithms. The numbered and filled circles represent the transducers, and the point at (x,y) represents a scattering site due to damage.

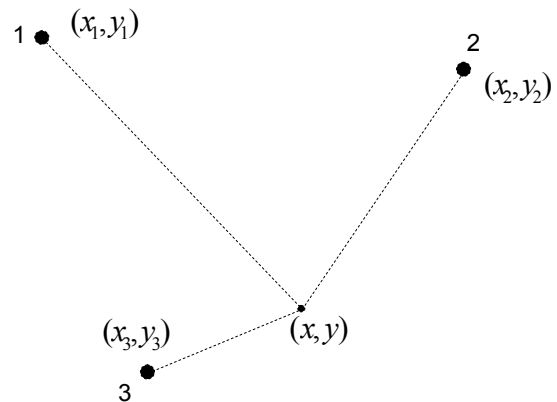


Fig. 1. Illustration of three transducers in a spatially distributed array. The point of interest (possible scattering site) is at (x,y) , and the various incident and scattered ray paths are shown as dashed lines.

A. Preprocessing of Received Signals

The broadband received signals are processed prior to imaging. The signals are first filtered by convolution with a 250 kHz, 3-cycle, Hanning-windowed tone burst to limit the frequency content. Next, the times of the direct transducer-to-transducer arrivals are measured, and the group velocity, c_g , is determined from the slope of the linear fit of the transducer-to-transducer distances to these arrival times. Signals are then windowed by multiplication with a decaying exponential starting at the time of the direct arrival to reduce the amplitude of more distant reflectors. That is,

$$w'(t) = w(t)e^{-(t-t_0)/t_d}; \quad t \geq t_0. \quad (1)$$

Here $w(t)$ is the filtered signal, t_0 is the time of the direct arrival, t_d is the exponential decay constant, and $w'(t)$ is the filtered and windowed signal (set to zero for $t < t_0$).

B. Arrival Time Algorithm

The arrival time algorithm is a delay-and-sum type method which accumulates the differenced signals from all transducer pairs using an appropriate delay law [4]. Sensor pair ij consists of the i th transducer located at (x_i, y_i) as transmitter and the j th transducer located at (x_j, y_j) as receiver. If there is damage located at (x, y) , the arrival time of the scattered signal at the receiver is the sum of the times for the incident wave to travel from the transmitter to the damage, and for the scattered signal to travel from the damage to the receiver,

$$t_{ij}(x, y) = \frac{\sqrt{(x_i - x)^2 + (y_i - y)^2} + \sqrt{(x_j - x)^2 + (y_j - y)^2}}{c_g}. \quad (2)$$

If $d_{ij}(t)$ is the differenced signal from sensor pair ij , then $d_{ij}(t_{ij}(x, y))$ corresponds to the amplitude of the signal scattered from the point (x, y) . The image value at (x, y) is the square of the sum over all $N(N-1)/2$ transducer pairs, where N is the total number of transducers,

$$E(x, y) = \left[\sum_{i=1}^{N-1} \sum_{j=i+1}^N d_{ij}(t_{ij}(x, y)) \right]^2. \quad (3)$$

From (2) and (3), it can be seen that a specific time point of the differenced signal is mapped to an ellipse with foci at the transducer locations. Note that $d_{ij}(t)$ can be either the raw (RF) signal, or the envelope-detected (rectified) signal.

C. Time Difference of Arrival Algorithm

The time difference of arrival algorithm considers transducers in groups of three with one acting as transmitter and the other two as receivers. If there is damage located at

the point (x, y) , then the difference in the times of arrival of the scattered signals at the two receivers is,

$$\Delta t_{ij}(x, y) = \frac{\sqrt{(x_i - x)^2 + (y_i - y)^2} - \sqrt{(x_j - x)^2 + (y_j - y)^2}}{c_g}, \quad (4)$$

where (x_i, y_i) and (x_j, y_j) are the coordinates of the two receivers. Since the distance from the transmitter to the damage is the same for both receivers, it does not affect the difference in arrival times. The image is constructed from the cross correlations of the various signal pairs,

$$E(x, y) = \sum_{n=1}^N \sum_{\substack{i=1 \\ i \neq n}}^{N-1} \sum_{\substack{j=i+1 \\ j \neq n}}^N x_{ni, nj}(\Delta t_{ij}(x, y)). \quad (5)$$

Here $x_{ni, nj}(t)$ is the cross correlation between the differenced signals from transducer pairs ni and nj (transducer n is the transmitter, and transducers i and j are receivers). There are a total of $N(N-1)(N-2)/2$ transducer triplets considered in the triple sum of (5). Either the raw (RF) or envelope-detected signals can be used to form the image $E(x, y)$, where the envelope detection is performed on the cross correlation result prior to implementation of (5).

III. EXPERIMENTS

A 6061 aluminum plate measuring 610 mm x 610 mm x 4.76 mm was instrumented with an array of six piezoelectric transducers fabricated from 12.5 mm diameter, 2.25 MHz, compressional mode PZT discs. The discs were enclosed in a brass housing, backed with epoxy, and bonded to the plate using conductive epoxy. Transducers were excited and signals received with a spike mode pulser receiver (Panametrics 5072PR), and a custom multiplexer switched between the 15 transmit-receive pairs. Signals were digitized at a frequency of 25 MHz and with a resolution of 10 bits, and 50 waveforms were averaged for each acquisition.

Because of the broadband excitation, multiple Lamb wave modes are generated in the plate. The dominant mode is S_0 , which has a strong peak close to 250 kHz. The initial filter significantly reduces all other modes except for A_0 since the cutoff frequency for the higher order modes is approximately 330 kHz. Considering these two modes, the expected range of group velocities is about 3 mm/ μ s to 5.5 mm/ μ s, which corresponds to plate transit times of about 100 μ s to 200 μ s.

The starting structural condition of the plate, which is considered to be the baseline condition for this work, included an area of simulated corrosion. A set of baseline signals were recorded under ambient laboratory conditions, and damage was introduced in the form of a 3 mm diameter through hole. A second set of signals was recorded from all transducers pairs after the hole was drilled, also under ambient conditions.

IV. RESULTS

The arrival time algorithm of Sec. IIB was applied to the differenced signals before and after the hole was drilled. Fig. 2 is the image constructed from the envelope-detected differenced signals with no exponential windowing. The transducer locations are indicated by the open circles, and the nominal hole location by a cross. Faint traces of the ellipse patterns are evident throughout the image, and there are artifacts near the plate edges due to the influence of the damage on the edge reflections. Fig. 3 is the same image of Fig. 2 but after exponential windowing with $t_d = 50 \mu\text{s}$. The windowing process essentially removes the later time signals arising from the edge reflections and thus eliminates the imaging artifacts near the plate edges.

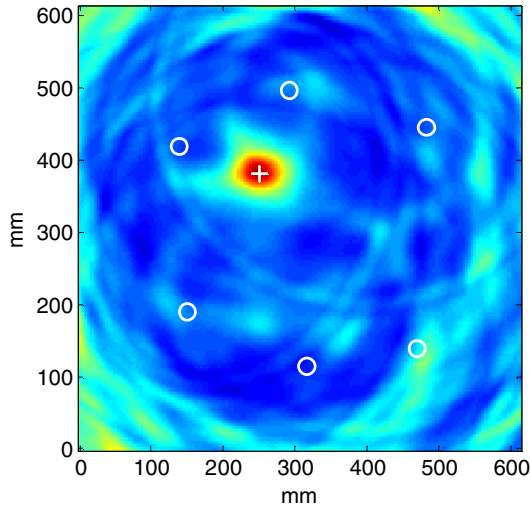


Fig. 2. Image based upon arrival times of scattered echoes applied to envelope detected differenced signals. Preprocessing consisted of filtering at 250 kHz and no exponential window.

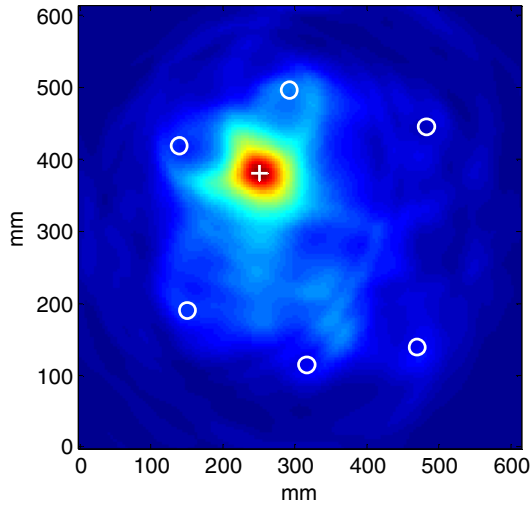


Fig. 3. Image based upon arrival times of scattered echoes applied to envelope detected differenced signals. Preprocessing consisted of filtering at 250 kHz and exponential windowing with $t_d = 50 \mu\text{s}$.

The time difference of arrival imaging method of Sec. IIC was applied to the same signals used to generate the previous images. Fig. 4 is the image constructed with no exponential windowing and with the cross correlations computed from the full time window of $500 \mu\text{s}$, which includes many edge reflections. The hyperbolic patterns are evident, and it is not clear whether the high intensity region near the actual defect location is an artifact or a spatially displaced indicator of the damage.

Fig. 5 is the image corresponding to Fig. 4 but with exponential windowing applied. The location of the defect is now clearly identified with only faint indications of the hyperbolic patterns in a generally uniform background. Note that all images are displayed using a linear color scale starting at zero.

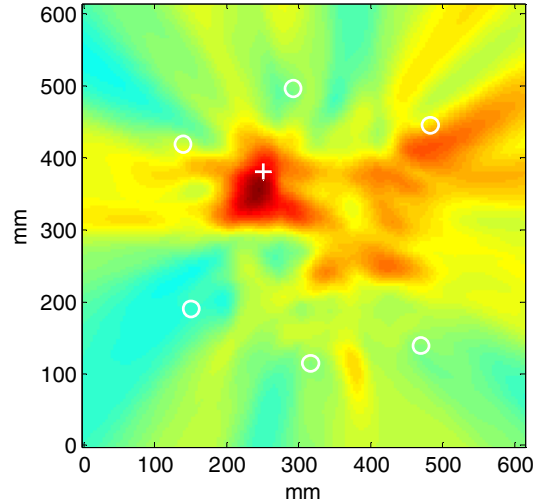


Fig. 4. Image based upon time difference of arrivals of scattered echoes applied to envelope detected cross correlations. Preprocessing consisted of filtering at 250 kHz and no exponential window.

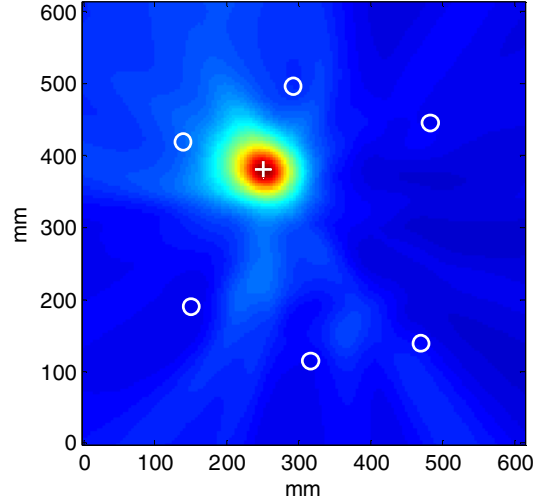


Fig. 5. Image based upon time difference of arrivals of scattered echoes applied to envelope detected cross correlations. Preprocessing consisted of filtering at 250 kHz and exponential windowing with $t_d = 50 \mu\text{s}$.

Images were also constructed from the RF waveforms with no envelope detection as shown in Figs. 6 and 7 for both imaging methods. The performance is very poor for the time of arrival method as is evident from Fig. 6. Although energy is somewhat concentrated in the vicinity of the damage location, there are multiple peaks and the actual location is not clearly indicated. For the time difference of arrival method, as shown in Fig. 7, the damage is now unambiguously located, although there are numerous lower amplitude artifacts in the background.

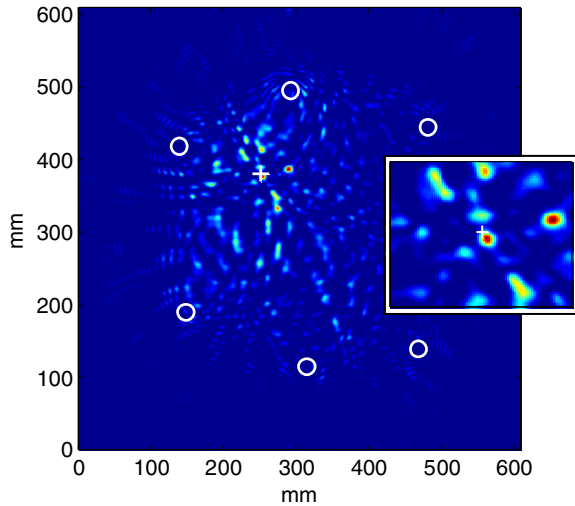


Fig. 6. Image based upon arrival times of scattered echoes applied to differenced signals without envelope detection (RF waveforms). Preprocessing consisted of filtering at 250 kHz and exponential windowing with $t_d = 50 \mu s$. The zoomed region is a 100 mm x 80 mm rectangle centered at the nominal defect location.

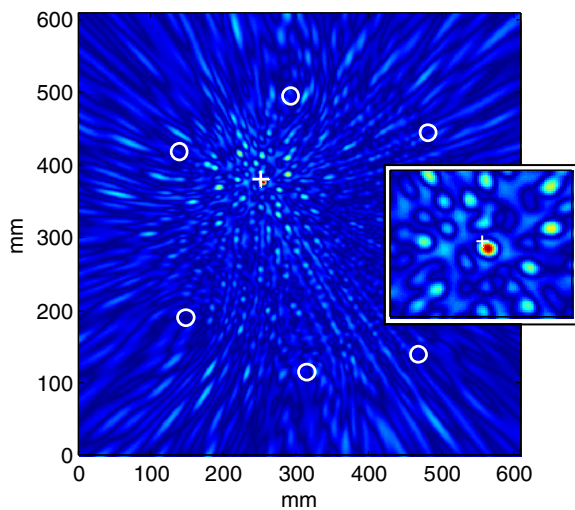


Fig. 7. Image based upon time difference of arrivals of scattered echoes applied to cross correlations without envelope detection (RF waveforms). Preprocessing consisted of filtering at 250 kHz and exponential windowing with $t_d = 50 \mu s$. The zoomed region is a 100 mm x 80 mm rectangle centered at the nominal defect location.

A further reduction in background artifacts can be achieved by considering multiple frequencies. Fig. 8 shows the result of averaging four images which were individually generated by filtering at 150 kHz, 200 kHz, 250 kHz and 300 kHz; each image was normalized to unity prior to averaging. The amplitude of the background artifacts is clearly reduced, resulting in a higher signal-to-noise ratio for the image of the damaged region.

V. DISCUSSION AND CONCLUSION

The results shown here indicate that both time of arrival and time difference of arrival algorithms can successfully image discrete damage in a plate from differenced signals using a spatially distributed array of ultrasonic sensors. The time of arrival method, which distributes the differenced signals in elliptical patterns, is effective even when edge reflections are present if performed using the envelope detected differenced signals. Application of an exponential window significantly reduces imaging artifacts resulting from edge reflections. When using unrectified RF differenced signals with this algorithm, imaging artifacts are severe with the damage causing multiple peaks of similar intensities.

The time difference of arrival method, which distributes cross correlations of differenced signals in hyperbolic patterns, is generally ineffective when edge reflections are present and windowing is not performed. In this case, the cross correlations are dominated by the larger amplitude and later time portions of the signals and do not capture time differences of arrival between the early scattered echoes. Exponential windowing significantly improves imaging, giving results similar to those produced by the time of arrival method.

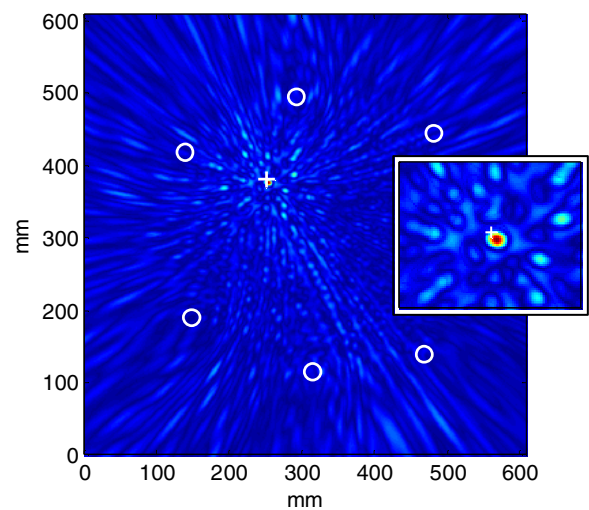


Fig. 8. Fused image generated from the average of four individual time difference of arrival images constructed at 150 kHz, 200 kHz, 250 kHz and 300 kHz; exponential windowing was applied with $t_d = 50 \mu s$. The zoomed region is a 100 mm x 80 mm rectangle centered at the nominal defect location.

Furthermore, for the experiment considered here, using unrectified RF cross correlation signals provided significantly improved damage localization at the expense of sizable imaging artifacts. The response from the damage was of higher intensity than the artifacts, enabling the damage to be unambiguously detected. The improved performance as compared to the time of arrival method is most likely due to the greater number of transducer combinations comprising the image (60 as compared to 15) as well as the insensitivity of the time difference of arrival algorithm to absolute time origins.

Additional reduction in artifact intensity was achieved by an image fusion process whereby images generated at multiple frequencies were normalized and averaged. Other fusion methods, such as a previously reported minimization algorithm [4], could also be applied. The image fusion process illustrates one possible means of effectively utilizing broadband signals in a dispersive environment.

Both the time of arrival and the time difference of arrival algorithms are based upon the differenced signals, and are thus dependent upon having signals and baselines which are well-matched. It is well-known that environmental effects such as temperature and surface conditions can significantly influence recorded signals, and this topic is the subject of current research [3,10]. Other effects, such as those due to long term aging, are not as well understood but must be addressed before a system based upon comparing signals to baselines can be implemented. Approaches which consider the nature of signal changes over time as well as the time scale of the changes should be considered so that benign aging effects can be discriminated from damage.

REFERENCES

- [1] X. Zhao, H. Gao, G. Zhang, B. Ayhan, F. Yan, C. Kwan, and J. Rose, "Active health monitoring of an aircraft with embedded piezoelectric sensor/actuator network: I. Defect detection, localization and growth monitoring," *Smart Mater. Struct.*, vol. 16, pp. 1208-1217, 2007.
- [2] C. Wang, J. T. Rose, and F.-K. Chang, "A synthetic time-reversal imaging method for structural health monitoring," *Smart Mater. Struct.*, vol. 13, pp. 415-423, 2004.
- [3] G. Konstantinidis, B. W. Drinkwater, and P. D. Wilcox, "The temperature stability of guided wave structural health monitoring systems," *Smart Mater. Struct.*, vol. 15, pp. 967-976, 2006.
- [4] J. E. Michaels and T. E. Michaels, "Guided wave signal processing and image fusion for *in situ* damage localization in plates," *Wave Motion*, vol. 44, pp. 482-492, 2007.
- [5] J. E. Michaels and T. E. Michaels, "Damage localization in inhomogeneous plates using a sparse array of ultrasonic transducers," *Rev. Prog. QNDE, AIP Proc.*, vol. 26A, pp. 846-853, 2007.
- [6] M. S. Brandstein, J. E. Adcock and H. F. Silverman, "A closed-form location estimator for use with room environment microphone arrays," *IEEE Trans. Speech Audio Processing*, vol. 5, no. 1, pp. 45-50, 1997.
- [7] J. Benesty, J. Chen and Y. Huang, "Time-delay estimation via linear interpolation and cross correlation," *IEEE Trans. Speech Audio Processing*, vol. 5, no. 1, pp. 509-519, 2004.
- [8] M. G. Baxter, R. Pullin, K. M. Holford and S. L., Evans, "Delta T source location for acoustic emission," *Mech. Sys. Sig. Proc.*, vol. 21, pp. 1512-1520, 2007.
- [9] H. Jeong and Y.-S. Jang, "Fracture source location in thin plates using the wavelet transform of dispersive waves," *IEEE Trans. Ultrason. Ferroelectr. Freq. Control*, vol. 47, no. 3, pp. 612-619, 2000.
- [10] Y. Lu and J. E. Michaels, "Consideration of surface variations on ultrasonic structural health monitoring," in *Proceedings of the 6th International Workshop on Structural Health Monitoring*, F.-K. Chang (Ed.), DEStech Publications, Inc., Lancaster, PA, pp. 1275-1282, 2007.